

# Mass dependence of nuclear shadowing at small Bjorken- $x$ from diffractive scattering

A. Adeluyi and G. Fai

*Center for Nuclear Research, Department of Physics  
Kent State University, Kent, OH 44242, USA*

(Dated: June 24, 2018)

We calculate the nuclear shadowing ratio for a wide range of nuclei at small Bjorken- $x$  in the framework of Gribov theory. The coherent contribution to the (virtual) photon-nucleon cross section is obtained in terms of the diffractive dissociation cross section. Information on diffraction from FNAL and HERA is used. Our results are compared to available data from the NMC and E665 experiments at  $x \simeq 10^{-4}$ .

PACS numbers: 24.85.+p, 25.30.Dh, 25.75.-q

## I. INTRODUCTION

Calculations of various cross sections in relativistic nucleus-nucleus collision physics in the framework of perturbative QCD (pQCD) require nuclear parton distribution functions (nPDFs). The nPDFs are usually presented in a parameterized form, as a product of free-nucleon PDFs and a “shadowing function” (see e.g. [1]), which depends on  $x$  and momentum transfer  $Q^2$ . Experimentally extracted shadowing functions are limited by the kinematic range of the data, and fits to these data do not provide the shadowing function in the whole requisite ( $x, Q^2$ ) region for all calculations.

Another approach is to utilize Gribov theory[2], which relates shadowing to diffraction. For the deuteron, the relationship involves the interaction of the diffractively scattered (virtual) photon with only two nucleons, but for heavy nuclei triple and higher-order scattering may be important and needs to be included in the formalism. This leads to some model dependence. For nuclear collision applications, nPDF uncertainties contribute significantly to the overall uncertainties of calculated quantities. Thus, an accurate determination of nPDFs is of paramount significance.

It is well-established experimentally that for small values of the Bjorken variable ( $x \lesssim 0.1$ ), the nuclear structure functions  $F_2^A$  are significantly reduced compared to  $A$  times the free nucleon structure function  $F_2^N$ , where  $A$  denotes the mass number of a specific nucleus. Equivalently, the virtual photon-nucleus cross section is less than  $A$  times the one for free nucleons,  $\sigma_{\gamma^*A} < A\sigma_{\gamma^*N}$ . This phenomenon became known as nuclear shadowing (in a strict sense). The same behavior is observed for real photons at sufficiently high energies ( $\nu \gtrsim 3$  GeV). Shadowing constitutes the most pronounced nuclear effect in lepton-nucleus deep inelastic scattering (DIS). (Note that in a generalized sense all modifications of the structure function in the entire range of  $x$ , including regions where  $F_2^A > A F_2^N$ , are sometimes referred to as “shadowing”.)

The shadowing ratio can be defined as  $F_2^A / (A * F_2^N)$ . Since the virtual photon-nucleus cross section is proportional to  $F_2$ , the shadowing ratio can be expressed alternatively as  $\sigma_{\gamma^*A} / (A * \sigma_{\gamma^*N})$ . In this work we employ Gribov theory, including the real part of the diffractive

scattering amplitude, to calculate the shadowing ratio at very small Bjorken- $x$ . We compare to experimental results from the NMC[3, 4] and E665[5, 6] experiments. These experimental data are all at small  $Q^2$ ; we thus use the information from diffractive scattering of real photons ( $Q^2 = 0$  GeV<sup>2</sup>).

The paper is organized as follows: in Sec. II we review the basic formalism of Gribov theory as applied to shadowing in the small Bjorken- $x$  regime. This is essentially the same treatment as described in Ref. [7], where the basic object is the diffractive structure function. Here the basic quantity is the differential diffractive cross section. Sec. III deals with diffractive production and the diffractive dissociation cross section. We present the results of our calculation in Sec. IV, and conclude in Sec. V.

## II. DIFFRACTION AND NUCLEAR SHADOWING

### A. Shadowing Ratio

Several natural length scales may become important in scattering off of a nucleus of mass number  $A$ . Most important for the present discussion is the average inter-nucleon separation,  $d$ , of the order of 2 fm. A high energy (virtual) photon scattered from the system can experience nuclear effects in two distinct ways[8]:

- i) incoherent scattering from  $A$  nucleons with modifications to the structure functions due to many-body effects in the nuclear medium;
- ii) coherent scattering processes involving more than one nucleon at a time.

The latter effects occur when hadronic excitations (or fluctuations) produced by the high-energy photon propagate over distances (in the laboratory frame) comparable to or larger than the characteristic length scale  $d \sim 2$  fm. Shadowing can be understood in terms of coherent scattering on more than one nucleon. Incoherent scattering occurs primarily in the range  $0.1 < x < 1$ , while strong coherence effects are manifest at  $x < 0.1$ .

The (virtual) photon-nucleus cross section can be separated into a part which accounts for the incoherent scattering from individual nucleons, and a correction (shadowing correction) from the coherent interaction with several nucleons:

$$\sigma_{\gamma^*A} = Z \sigma_{\gamma^*p} + (A - Z) \sigma_{\gamma^*n} + \delta\sigma_{\gamma^*A} . \quad (1)$$

The single scattering part is the incoherent sum of photon-nucleon cross sections, where  $Z$  is the nuclear charge number, and  $\sigma_{\gamma^*p}$  and  $\sigma_{\gamma^*n}$  are the photon-proton and photon-neutron cross sections, respectively. The multiple scattering correction can be viewed as expanded in terms of the number of nucleons in the target involved in the coherent scattering ( $n \geq 2$ ). The leading contribution to nuclear shadowing comes from double scattering, since the probability that the propagating hadronic excitation coherently interacts with several nucleons decreases with the number of nucleons. For the deuteron, only the double-scattering term ( $n = 2$ ) is present.

We define the shadowing ratio as

$$\mathcal{R}_A^S = \frac{Z \sigma_{\gamma^*p} + (A - Z) \sigma_{\gamma^*n} + \delta\sigma_{\gamma^*A}}{Z \sigma_{\gamma^*p} + (A - Z) \sigma_{\gamma^*n}} . \quad (2)$$

Thus, the evaluation of the shadowing correction,  $\delta\sigma_{\gamma^*A}$ , is central to the calculation of the shadowing ratio. In the next section we utilize the Gribov theory in a generalized form to determine  $\delta\sigma_{\gamma^*A}$ .

### B. Shadowing Correction From Generalized Gribov Theory

The Gribov theory highlights the deep connection between nuclear shadowing and diffraction. The original formulation relates the correction to the cross section in hadron-deuteron scattering to diffraction off of a nucleon. For the deuteron (and other light nuclei where double scattering is dominant), the shadowing correction can be evaluated without any ambiguity associated with the involvement of more than two target nucleons. For heavier nuclei, one needs to go beyond double scattering. Multiple scattering with  $n > 2$  nucleons may contribute significantly to the shadowing correction (depending on the kinematic regime). These contributions are not model-independent; therefore the evaluation of the shadowing correction using Gribov formalism depends to some extent on the model for the  $n > 2$  multiple scattering.

The original formulation by Gribov neglects the real part of the diffractive scattering amplitude. Here we take this into account and denote by  $\eta$  the ratio of the real to imaginary parts of the diffractive scattering amplitude. In the generalized form incorporating the real part, the shadowing correction at the level of double scattering is

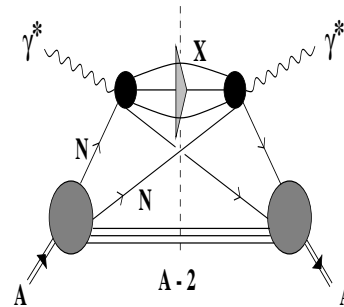


FIG. 1: Double scattering contribution to nuclear DIS.

given by

$$\delta\sigma_{\gamma^*A} = \frac{A(A-1)}{2A^2} 16\pi \mathcal{R} e \left[ \frac{(1-i\eta)^2}{1+\eta^2} \int d^2b \int_{-\infty}^{\infty} dz_1 \int_{z_1}^{\infty} dz_2 \int_{4m_\pi^2}^{W^2} dM_X^2 \left. \frac{d^2\sigma_{\gamma^*N}^{\text{diff}}}{dM_X^2 dt} \right|_{t \approx 0} \rho_A^{(2)}(\vec{b}, z_1; \vec{b}, z_2) \exp \left\{ i \frac{(z_1 - z_2)}{\lambda} \right\} \right] . \quad (3)$$

Here  $\sigma_{\gamma^*N}^{\text{diff}}$  is the photon-nucleon diffractive cross section and  $z$  represents the beam direction. The coherence length,  $\lambda$ , is given by  $\lambda = 2\nu/M_X^2$  for real photons. As illustrated in Fig. 1, a diffractive state with invariant mass  $M_X$  is produced in the interaction of the photon with a nucleon located at position  $(\vec{b}, z_1)$  in the target. The hadronic excitation is assumed to propagate at fixed impact parameter  $\vec{b}$  and to interact with a second nucleon at  $z_2$ . The probability to find two nucleons in the target at the same impact parameter is described by the two-body density  $\rho_A^{(2)}(\vec{b}, z_1; \vec{b}, z_2)$  normalized as  $\int d^3r d^3r' \rho_A^{(2)}(\vec{r}, \vec{r}') = A^2$ . The phase factor,  $\exp \{i[(z_1 - z_2)/\lambda]\}$  in eq. (3) implies that only diffractively excited hadrons with a longitudinal propagation length larger than the average nucleon-nucleon distance in the target,  $\lambda > d \simeq 2$  fm, can contribute significantly to double scattering. The limits of integration define the kinematically permitted range of diffractive excitations, with their invariant mass  $M_X$  above the two-pion production threshold and limited by the center-of-mass energy  $W = \sqrt{s}$  of the scattering process.

In order to approximate the two-body density  $\rho_A^{(2)}(\vec{b}, z_1; \vec{b}, z_2)$ , we note that short-range nucleon-nucleon correlations are relevant in nuclei when  $z_2 - z_1$  is comparable to the range of the short-range repulsive part of the nucleon-nucleon force, i.e. for distances  $\lesssim 0.4$  fm. However, shadowing is negligible in this case. Short-range correlations are therefore not important in the shadowing domain, and the target can be considered as an ensemble of independent nucleons with  $\rho_A^{(2)}(\vec{r}, \vec{r}') \approx \rho_A(\vec{r})\rho_A(\vec{r}')$ , where  $\rho_A$  is the nuclear one-body density.

With increasing photon energies or decreasing  $x$  down

to  $x \ll 0.1$ , the longitudinal propagation length of diffractively excited hadrons rises and eventually reaches nuclear dimensions. Thus, for heavy nuclei interactions of the excited hadronic state with several nucleons in the target become important and should be accounted for. Following [7] we introduce an attenuation factor with an effective hadron-nucleon cross section,  $\sigma_{\text{eff}}$ . The shadowing correction can thus be written as

$$\delta\sigma_{\gamma^*A} = \frac{A(A-1)}{2A^2} 16\pi \mathcal{R}e \left[ \frac{(1-i\eta)^2}{1+\eta^2} \int d^2b \int_{-\infty}^{\infty} dz_1 \int_{z_1}^{\infty} dz_2 \int_{4m_\pi^2}^{W^2} dM_X^2 \frac{d^2\sigma_{\gamma^*N}^{\text{diff}}}{dM_X^2 dt} \Big|_{t \approx 0} \rho_A^{(2)}(\vec{b}, z_1; \vec{b}, z_2) \exp \left\{ i \frac{(z_1 - z_2)}{\lambda} \right\} \exp \left\{ -(1/2)(1-i\eta)\sigma_{\text{eff}} \int_{z_1}^{z_2} dz \rho_A(b, z) \right\} \right]. \quad (4)$$

The effective hadron-nucleon cross section,  $\sigma_{\text{eff}}$  in eq. (4) is defined as

$$\sigma_{\text{eff}} = \frac{16\pi}{\sigma_{\gamma N}(1+\eta^2)} \int_{4m_\pi^2}^{W^2} dM_X^2 \frac{d^2\sigma_{\gamma^*N}^{\text{diff}}}{dM_X^2 dt} \Big|_{t \approx 0}, \quad (5)$$

where  $\sigma_{\gamma N}$  is the photon-nucleon cross section. The details of this approach and the approximations inherent in the definition of  $\sigma_{\text{eff}}$  are treated thoroughly in [7]. For vector mesons as the intermediate hadronic excitations, we take  $\sigma_{VN}$  as  $\sigma_{\text{eff}}$  in the attenuation factor in eq. (4), where  $\sigma_{VN}$  is the vector meson-nucleon scattering cross section.

When  $x \ll 0.1$ , it is a good approximation to ignore the phase factor,  $\exp i[(z_1 - z_2)/\lambda]$ , in eq. (4), and (using Leibnitz's rule) the integrals over  $z_1$  and  $z_2$  can be carried out explicitly. This leads to a simplified form,

$$\delta\sigma_{\gamma^*A} = \frac{2(1-1/A)\sigma_{\gamma N}}{\sigma_{\text{eff}}} \mathcal{R}e \left( \int d^2b \left[ \exp \{-LT(b)\} - 1 + LT(b) \right] \right), \quad (6)$$

where  $L = (A/2)(1-i\eta)\sigma_{\text{eff}}$  and  $T(b) = \int_{-\infty}^{\infty} dz \rho_A(b, z)$ , the usual Glauber thickness function. However, we use the full expression, eq. (4), in our calculation.

Eq. (4) gives the shadowing correction in terms of  $\sigma_{\text{eff}}$ . This effective cross section involves the differential diffractive dissociation cross section at small  $t$ , see eq. (5). The treatment of this diffractive cross section is the subject of the next section.

### III. DIFFRACTIVE DISSOCIATION

#### A. Diffractive production

Consider the single diffractive scattering of a (virtual) photon off of a proton (see Fig. 2). The proton does not

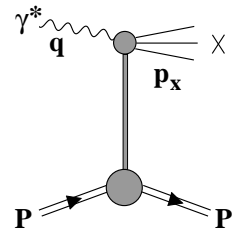


FIG. 2: Diffractive scattering from a proton.

dissociate, and it remains intact during the process. The photon, on the other hand, dissociates into a hadronic final state  $X$ , which is well separated in rapidity from the proton,

$$\gamma^{(*)} + p \rightarrow X + p'. \quad (7)$$

Such diffractive processes are important at small momentum transfer, with cross sections which decrease exponentially with the squared four-momentum transfer. In general they exhibit a weak energy dependence.

Diffractive dissociation of real photons,

$$\gamma + N \rightarrow X + N, \quad (8)$$

has been studied in both fixed target and collider experiments. Experiments were carried out at Fermi National Laboratory (FNAL) at average photon-proton center of mass energies of  $W \simeq 12.9$  GeV and  $W \simeq 15.3$  GeV[9]. Diffractive states with an invariant mass squared of up to  $M_X^2 \simeq 18$  GeV<sup>2</sup> were produced. This experiment measured the diffractive dissociation cross section differential in both, the invariant mass  $M_X$  and the squared four-momentum transfer  $t$ . Experiments at the Hadron-Electron Ring Accelerator (HERA)[10, 11, 12, 13, 14] were carried out at average energies  $W \simeq 187$  GeV and  $W \simeq 231$  GeV. Diffractive states with mass  $M_X < 30$  GeV were produced. Unlike the FNAL experiment, only  $d\sigma_{\gamma^*N}^{\text{diff}}/dM_X^2$  was measured due to poor resolution in  $t$ .

As mentioned earlier, the available experimental data on shadowing at small  $x$  ( $x \simeq 10^{-4}$ ) are all at small  $Q^2$  ( $Q^2 < 1$  GeV<sup>2</sup>). At such small virtualities the photons can be considered quasi-real, and it is thus not a bad approximation to regard them as real photons with  $Q^2 = 0$  GeV<sup>2</sup>. The center-of-mass energies are also low:  $W \simeq 15$  GeV for the NMC and  $W \simeq 25$  GeV for the E665 measurements. These energies are comparable to the photon-proton center of mass energies at FNAL. For these reasons one can use the information from diffractive scattering of real photons at FNAL to calculate the shadowing ratio in the kinematic range accessible at NMC and E665.

#### B. Diffractive dissociation cross section

It is natural to divide the diffractive dissociation cross section data as a function of  $M_X^2$  into the region of the

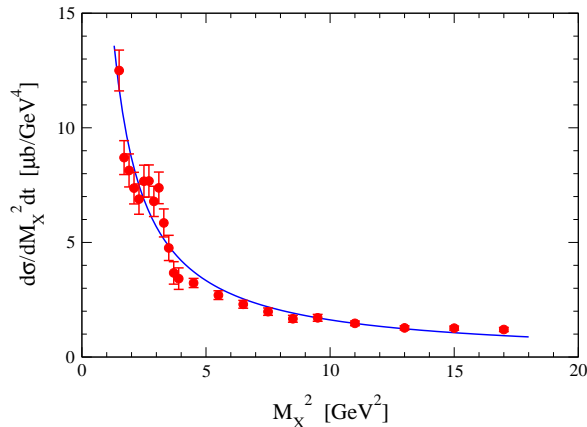


FIG. 3: (Color Online) Triple-pomeron fit to the FNAL data[9], including the  $\rho'$  resonances in the continuum, as in Ref. [15].

low-mass vector mesons ( $\rho$ ,  $\omega$ , and  $\phi$ ) and a high-mass continuum, with a matching point of  $M_X^2 \simeq 2.25 \text{ GeV}^2$ , as in Ref. [15]. However, in this case a triple-pomeron fit to the continuum data (as described in Sec. III B 3) misses the  $\rho'$  resonances as can be seen in Fig. 3.

The analysis by the H1 collaboration[10] divides the HERA photoproduction data into effectively three intervals in  $M_X^2$ . We follow this strategy in the present paper, taking the first interval (0.16 – 1.58)  $\text{GeV}^2$  to contain the region of the low-mass vector mesons ( $\rho$ ,  $\omega$  and  $\phi$ ). The second interval (1.58 – 4.0  $\text{GeV}^2$ ) covers the  $\rho'$  resonance region. The third interval ( $M_X^2 > 4.0 \text{ GeV}^2$ ) is that of the high-mass continuum. The differential diffractive cross section is thus written as a sum over contributions from these three mass intervals,

$$\left. \frac{d\sigma_{\gamma N}^D}{dM_X^2 dt} \right|_{t \approx 0} = \sum_{V=\rho, \omega, \phi} \left. \frac{d\sigma_{\gamma N}^V}{dM_X^2 dt} \right|_{t \approx 0} + \sum_{V=\rho'} \left. \frac{d\sigma_{\gamma N}^V}{dM_X^2 dt} \right|_{t \approx 0} + \left. \frac{d\sigma_{\gamma N}^{\text{cont}}}{dM_X^2 dt} \right|_{t \approx 0}. \quad (9)$$

In the following, we briefly summarize the various approximations applied in the three regions.

### 1. Low-mass vector mesons

Generalized vector meson dominance (VMD) [16] can be utilized to describe the contribution of the low-mass vector mesons to the differential diffractive cross section, i.e. the first term on the right-hand side of eq. (9):

$$\left. \frac{d\sigma_{\gamma N}^V}{dM_X^2 dt} \right|_{t \approx 0} = \frac{e^2}{16\pi} \frac{\Pi^V(M_X^2)}{M_X^2} \sigma_{VN}^2. \quad (10)$$

with  $\Pi^V(M_X^2)$  the vector meson part of the photon spectral function  $\Pi(M_X^2)$ , which is given by

$$\Pi(M_X^2) = \frac{1}{12\pi^2} \frac{\sigma(e^+e^- \rightarrow \text{hadrons})}{\sigma(e^+e^- \rightarrow \mu^+\mu^-)}. \quad (11)$$

In eq. (10),  $\sigma_{VN}$  is the vector meson-nucleon cross section and  $e^2/4\pi = 1/137$  is the fine structure constant. The  $\omega$  and  $\phi$  mesons are narrow and thus well approximated by delta functions. One can write their contribution to the photon spectral function as

$$\Pi^V(M_X^2) = \left( \frac{m_V}{g_V} \right)^2 \delta(M_X^2 - m_V^2); \quad V = \omega, \phi, \quad (12)$$

where  $m_V$  and  $g_V$ , ( $V = \omega, \phi$ ) are the mass and the coupling constant of the  $\omega$  and  $\phi$  mesons, respectively.

The  $\rho$ -meson, unlike the  $\omega$  and  $\phi$  mesons, has a large width due to its strong coupling to two-pion states. We have followed the approach in [15] and taken this into account through the  $\pi^+\pi^-$  part of the photon spectral function:

$$\Pi^\rho(M_X^2) = \frac{1}{48\pi^2} \Theta(M_X^2 - 4m_\pi^2) \left( 1 - \frac{4m_\pi^2}{M_X^2} \right)^{3/2} |F_\pi(M_X^2)|^2, \quad (13)$$

where  $m_\pi$  is the mass of the pion and  $M_X = M_{\pi\pi}$  is the invariant mass of the  $\pi^+\pi^-$  pair. The pion form factor,  $F_\pi$  is taken from Ref. [17]. A full discussion is given in [15]. We compared the result from the delta function approximation to this more exact calculation and found that taking into account the width of the  $\rho$ -meson increases the differential diffractive cross section by 10%.

The vector meson-nucleon cross section in eq. (10) has an energy dependence of the form

$$\sigma_{VN} \sim W^{2(\alpha_{\mathbb{P}}(0)-1)} = W^{2\epsilon} \quad (14)$$

where  $\alpha_{\mathbb{P}}(t=0) = 1 + \epsilon$  is the soft pomeron intercept[18].

### 2. Region of the $\rho'$ resonances

The  $\rho'$  resonance region contains the  $\rho(1450)$  and  $\rho(1700)$  mesons. These resonances were formerly classified as the  $\rho(1600)$  [19]. In Ref. [15] the  $\rho'$  resonance region is lumped together with the high-mass continuum. As can be seen in Fig. 3, the FNAL data show an enhancement in this region. We treat this enhancement in terms of an average  $\rho'$  resonance, corresponding to the earlier classification of  $\rho(1600)$ , as done in Ref. [9]. We use the available information on the  $\rho(1600)$  from Ref. [16] in a VMD-type calculation to evaluate the contribution from this region. The average  $\rho'$  resonance should have a finite width, but encouraged by the fact that a

delta function in the case of the  $\rho$  gives a good approximation to the full-width result, we employ a narrow resonance approximation for the  $\rho(1600)$ . Thus, for the second term of (9) we have

$$\left. \frac{d\sigma_{\gamma N}^V}{dM_X^2 dt} \right|_{t \approx 0} = \frac{e^2}{16\pi} \frac{\Pi^V(M_X^2)}{M_X^2} \sigma_{VN}^2. \quad (15)$$

with

$$\Pi^V(M_X^2) = \left( \frac{m_V}{g_V} \right)^2 \delta(M_X^2 - m_V^2) \quad (16)$$

and  $V = \rho(1600)$ .

### 3. High-mass continuum

A full treatment of both the FNAL data and the HERA data in this region has been carried out by the H1 Collaboration in Ref. [10], using the triple-Regge model of photon dissociation. For simplicity we consider only the triple-pomeron term, ignoring the sub-leading reggeons and interference between the pomeron and reggeons. In this case the differential dissociation cross section can be written as

$$\frac{d^2\sigma}{dM_X^2 dt} = \frac{G_{\mathbb{P}\mathbb{P}\mathbb{P}}(0)}{s_0^{\alpha_{\mathbb{P}}(0)-1}} (W^2)^{2\alpha_{\mathbb{P}}(0)-2} \left( \frac{1}{M_X^2} \right)^{\alpha_{\mathbb{P}}(0)} e^{B(W^2, M_X^2) t}, \quad (17)$$

where  $s_0$  is the hadronic mass scale and  $B(W^2, M_X^2) = 2b_{p\mathbb{P}} + b_{\mathbb{P}\mathbb{P}\mathbb{P}} + 2\alpha'_{\mathbb{P}} \ln W^2/M_X^2$ . Here  $b_{p\mathbb{P}}$  is the proton-pomeron slope parameter,  $b_{\mathbb{P}\mathbb{P}\mathbb{P}}$  the triple pomeron slope parameter, and  $\alpha'_{\mathbb{P}}$  is the slope of the pomeron trajectory. We use the values in [10] for these parameters, with  $s_0 = 1 \text{ GeV}^2$ .

In order to have a consistent treatment of the different contributions, we take  $\alpha_{\mathbb{P}}(0) = 1.068 \pm 0.0492$  from [10]. This agrees within error with the soft pomeron intercept in Ref. [18] ( $\alpha_{\mathbb{P}}(0) \simeq 1.081$ ). Thus the only free parameter is the triple-pomeron coupling  $G_{\mathbb{P}\mathbb{P}\mathbb{P}}(0)$ . We fit the FNAL data at the average energy  $W = 14.3 \text{ GeV}$  and  $t = -0.05 \text{ GeV}$  to eq. (17). The fit gives  $G_{\mathbb{P}\mathbb{P}\mathbb{P}}(0) = 11.4 \text{ mb/GeV}^{2(1+\epsilon)}$ . The quality of our fit is shown in Fig. 4.

## IV. RESULTS

The treatment outlined in the last two sections is now applied to calculate the shadowing correction, and hence the shadowing ratio. The basic equation is eq. (6), which involves the ratio of the real to imaginary amplitudes  $\eta$ , the photon-nucleon cross section  $\sigma_{\gamma N}$ , the nuclear density  $\rho_A$ , and the effective cross section  $\sigma_{\text{eff}}$ .

We use the energy-independent  $\eta$ 's for the vector mesons from Ref. [16]. For both  $\rho$  and  $\omega$  mesons,  $\eta$  takes

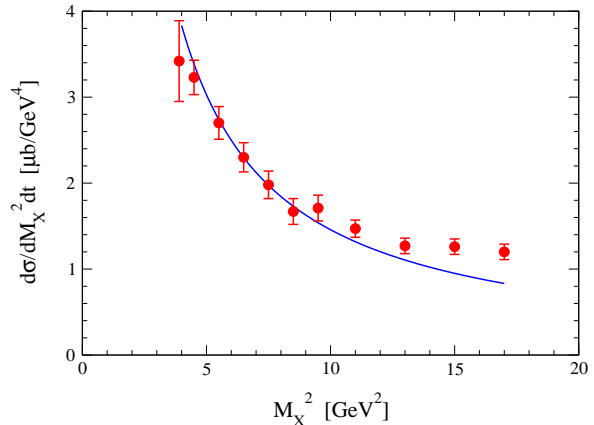


FIG. 4: (Color Online) Triple pomeron fit to the FNAL[9] data in the nonresonant continuum ( $M_X^2 > 4 \text{ GeV}^2$ ).

values between 0 and  $-0.3$ . Here we take  $\eta_\rho = \eta_\omega = -0.2$  in accordance with Ref. [16]. The results of our calculation are not very sensitive to the precise values of  $\eta_{\rho(\omega)}$ . For the  $\phi$  meson, we take  $\eta_\phi = 0.13$  [20]. For lack of information, we take  $\eta_{\rho(1600)} = 0$ . For the high-mass continuum, we follow Ref. [7] and define  $\eta_{\text{cont}}$  as

$$\eta_{\text{cont}} = \frac{\pi}{2} (\alpha_{\mathbb{P}}(0) - 1), \quad (18)$$

using the result of Gribov and Migdal [21].

The small difference between the photon-proton cross section  $\sigma_{\gamma p}$  and the photon-neutron cross section  $\sigma_{\gamma n}$  is neglected in this study. We use the Donnachie-Landshoff parameterization of  $\sigma_{\gamma p}$  [18] as the generic photon-nucleon cross section  $\sigma_{\gamma N}$ . For the nuclear densities three-parameter Fermi ( $3pF$ ) distributions are applied:

$$\rho(r) = \rho_0 \frac{1 + \omega(r/R_A)^2}{1 + e^{(r-R_A)/d}}, \quad (19)$$

with the parameter values taken from Ref. [22]. For mass numbers  $A \lesssim 20$  a harmonic oscillator (HO) density distribution may be more appropriate than the  $3pF$  distribution. For uniformity, we use the  $3pF$  distributions for the whole mass range in light of the fact that uncertainties associated with other parameters are at least comparable.

We carried out calculations at  $W = 15$  and  $25 \text{ GeV}$ , the approximate energies of the NMC and E655 experiments, respectively. The results are displayed in Fig. 5, together with the experimental data points. At very small  $x$  ( $x \simeq 10^{-4}$ ), NMC has two data points, corresponding to  ${}^6\text{Li}$  and  ${}^{12}\text{C}$ . The E665 experiment has four data points:  ${}^{12}\text{C}$ ,  ${}^{40}\text{Ca}$ ,  ${}^{131}\text{Xe}$ , and  ${}^{208}\text{Pb}$ . In view of the large error bars of the data, the calculation can be said to describe the experimental information in the entire mass range at E665 energies, and also for the two

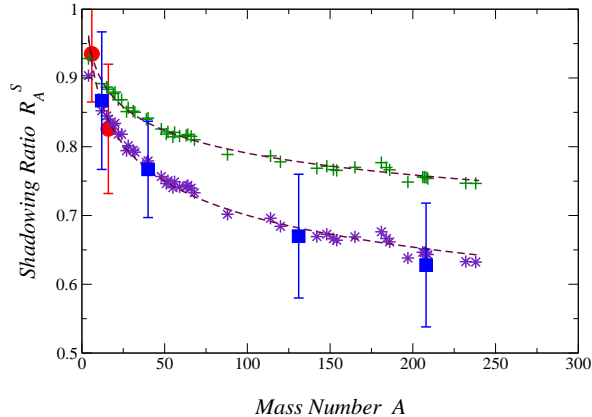


FIG. 5: (Color Online) Shadowing ratio calculated at  $W = 15$  GeV (crosses) and  $W = 25$  GeV (stars). Data are from the NMC (shaded circles) and E665 (shaded boxes) collaborations. The NMC point corresponding to  $^{12}\text{C}$  is displaced slightly for better visibility. The dashed lines are energy-dependent fits according to (20) as described in the text.

available data points at NMC energies. For small  $A$  the shadowing ratio decreases rapidly with  $A$ , while for large  $A$  the decrease is more gradual. The calculated result also falls steeply with increasing  $W$ .

The dashed lines in Fig. 5 represent a two-parameter fit of the standard form

$$\mathcal{R}_A^S = \beta_0 A^{\beta_1 - 1} \quad (20)$$

to the calculated results, with energy-dependent parameters  $\beta_0$  and  $\beta_1$ . In order to determine the energy dependence of the fit parameters we calculated the shadowing ratio for  $W$  in the range  $10 \leq W \leq 30$  GeV. The energy dependence of the fit coefficients can be described as

$$\beta_0 = 0.720 + 0.118 \ln(W) \quad (21)$$

and

$$\beta_1 = 1.143 - 0.075 \ln(W), \quad (22)$$

where  $W$  is the center-of-mass energy in GeV.

The fit does very well for the entire mass range for low  $W$  and deviates from the calculated result at large

$A$  as  $W$  increases. This seems to suggest that the mass dependence of the calculated shadowing ratio at large  $A$  and increasing  $W$  is not as simple as in eq. (20). A five-parameter fourth-degree polynomial with energy-dependent coefficients gives a good fit for the entire mass range and at all energies considered. However, we prefer the simple physical picture of the two-parameter fit, which is adequate considering the experimental and theoretical error bars.

The uncertainties of our calculation are mostly related to the various parameterizations of the diffractive dissociation cross section. The delta function parameterization for the  $\omega$  and  $\phi$  mesons should be satisfactory, and the width of the  $\rho$  meson has been taken into account. Refinements of the spectral function (13) are possible, and improvements of the treatment of the  $\rho'$  resonance region is also left for future work. The uncertainties in the continuum are associated with the neglect of sub-leading reggeons and of interference terms. Furthermore, the use of an effective scattering cross section to account for multiple scattering is an approximation, as is using real-photon information ( $Q^2 = 0$ ) at small, but non-vanishing  $Q^2$ . We estimate the overall uncertainty of our calculated results to be in the 20% range.

## V. CONCLUSION

We have calculated the shadowing ratio at very small Bjorken- $x$  for nuclei in the range  $3 < A < 239$  using Gribov theory. We included the effect of the real part of the diffractive scattering amplitude. The photon diffractive dissociation cross section, which serves as an input to our calculation, was parameterized as a function of the invariant mass of the diffractively produced hadronic excitation using vector meson dominance and Regge theory in three mass intervals: low-mass vector mesons,  $\rho'$  resonances, and continuum. The parameters needed are taken from earlier studies that fit experimental data.

It is found that the calculated shadowing ratio decreases with mass number first rapidly and then more slowly. To be able to compare to NMC/E665 data, the calculations are all at low center-of-mass energy, and the decrease with  $A$  is stronger as the center-of-mass energy increases. We find that Gribov theory gives a reasonable estimate of the mass dependence of nuclear shadowing at small Bjorken- $x$ .

- 
- [1] K. J. Eskola, V. J. Kolhinen and C. A. Salgado, Eur. Phys. J. C **9**, 61 (1999).  
 [2] V. N. Gribov, Sov. Phys. JETP **30**, 709 (1970) [Zh. Eksp. Teor. Fiz. **57**, 1306 (1969)].  
 [3] P. Amaudruz *et al.* [New Muon Collaboration], Nucl. Phys. B **441**, 3 (1995).  
 [4] M. Arneodo *et al.* [New Muon Collaboration], Nucl.

- Phys. B **441**, 12 (1995).  
 [5] M. R. Adams *et al.* [E665 Collaboration], Phys. Rev. Lett. **68**, 3266 (1992).  
 [6] M. R. Adams *et al.* [E665 Collaboration], Z. Phys. C **67**, 403 (1995).  
 [7] L. Frankfurt, V. Guzey and M. Strikman, Phys. Lett. B **586**, 41 (2004).

- [8] G. Piller and W. Weise, Phys. Rept. **330**, 1 (2000).
- [9] T. J. Chapin *et al.*, Phys. Rev. D **31**, 17 (1985).
- [10] C. Adloff *et al.* [H1 Collaboration], Z. Phys. C **74**, 221 (1997).
- [11] J. Breitweg *et al.* [ZEUS Collaboration], Eur. Phys. J. C **2**, 237 (1998).
- [12] J. Breitweg *et al.* [ZEUS Collaboration], Z. Phys. C **75**, 421 (1997).
- [13] S. Aid *et al.* [H1 Collaboration], Z. Phys. C **69**, 27 (1995).
- [14] M. Derrick *et al.* [ZEUS Collaboration], Z. Phys. C **63**, 391 (1994).
- [15] G. Piller, G. Niesler and W. Weise, Z. Phys. A **358**, 407 (1997).
- [16] T. H. Bauer, R. D. Spital, D. R. Yennie and F. M. Pipkin, Rev. Mod. Phys. **50**, 261 (1978) [Erratum-ibid. **51**, 407 (1979)].
- [17] F. Klingl, N. Kaiser and W. Weise, “Effective Lagrangian approach to vector mesons, their structure and Z. Phys. A **356**, 193 (1996).
- [18] A. Donnachie and P. V. Landshoff, Phys. Lett. B **296**, 227 (1992).
- [19] K. Hagiwara *et al.* [Particle Data Group], Phys. Rev. D **66**, 010001 (2002).
- [20] L. Frankfurt, G. Piller, M. Sargsian and M. Strikman, Eur. Phys. J. A **2**, 301 (1998).
- [21] V. N. Gribov and A. A. Migdal, “Properties of the pomeron pole and the branch cuts related to it at low Sov. J. Nucl. Phys. **8**, 583 (1969) [Yad. Fiz. **8**, 1002 (1968)].
- [22] C. W. De Jager, H. De Vries and C. De Vries, Atom. Data Nucl. Data Tabl. **14**, 479 (1974).